Aluminium salabza complexes for fixation of CO_2 to organic carbonates

Supplementary Information

L. Cuesta-Aluja,* J. Castilla and A. M. Masdeu-Bultó*

Department of Physical and Inorganic Chemistry. University Rovira i Virgili. Marcel·lí Domingo, s/n. 43007 Tarragona (Spain).

Experimental section

General considerations

H_2L was prepared following described procedures.[1] All complexes were prepared using Schlenk technique under inert conditions. Epoxides were dried over CaH_2, distilled and stored under inert atmosphere except 1,2-epoxyhexane, 1,2-epoxydodecane and 1-chloro-2,3-epoxypropane, which were purchased at Sigma-Aldrich and used as received. Solvents were purified by the system Braun MB SPS-800 and stored under nitrogen atmosphere. Carbon dioxide (SCF Grade, 99.999 %, Air Products) was used introducing an oxygen/moisture trap in the line (Agilent). IR spectra were recorded on a Midac Grams/386 spectrometer in ATR (range 4000-600) cm^{-1} or KBr range (4000- 400 cm^{-1}). UV-visible spectra were recorded on a UV-3100PC spectrophotometer. NMR spectra were recorded at 400 MHz Varian, with peaks from solvent as references (^{1}H NMR, ^{13}C NMR) and aluminum nitrate (^{27}Al NMR) as external reference. Electrospray ionization mass spectra (ESI-MS) were obtained with an Agilent Technologies mass spectrometer. Typically, a dilute solution of the compound in the indicated solvent (1:99) was delivered directly to the spectrometer source at 0.01 ml·min^{-}1 with a Hamilton microsyringe controlled by a single-syringe infusion pump. The nebulizer tip operated at 3000–3500 V and 250 °C, and nitrogen was both the drying and a nebulizing gas. The cone voltage was 30 V. Quasi-molecular ion peaks $[M-H]^-$ (negative ion mode) or sodiated $[M + Na]^+$ (positive ion mode) peaks were assigned on the basis of the *m/z* values. MALDI-TOF measurements of polymers were performed on a Voyager-DE-STR (Applied Biosystems) instrument equipped with a 337 nm nitrogen laser. All spectra were acquired in the positive ion reflector mode. Dithranol was used as matrix, which was dissolved in MeOH at a concentration of 10 mg·mL^{-1}. The polymer (5 mg) was dissolved in 1 mL of $CHCl_3$. 1µl of sample, 1µl of matrix and 1µl of potassium trifluoroacetate (KTFA) solution (1 mg of KTFA in 1ml of THF) were deposited consecutively on the stainless steel sample holder and allowed to dry before introduction into the mass spectrometer. Three independent measurements were made for each sample. For each spectrum 100 laser shots were accumulated. The molecular weights (M_w) of copolymers and the molecular weight distributions (M_w/M_n) were determined by gel permeation chromatography versus polystyrene standards. Measurements were made in THF on a Millipore-Waters 510 HPLC Pump device using three-serial column system (MZ-Gel 100Å, MZ-Gel 1000 Å, MZ-Gel 10000 Å linear columns) with UV-Detector (ERC-7215) and IR-Detector (ERC-7515a). The software used to get the data was NTeqGPC 5.1. Samples were prepared as follow: 5 mg of the copolymer were dissolved with 2 ml of tetrahydrofuran (HPLC grade) and using toluene (HPLC grade) as internal standard. Magnetic susceptibilities were measured on a Sherwood MSBmk1 magnetic susceptibility balance with KK105 as a calibration standard. Elemental analyses were performed at the Serveis Tècnics de Recerca from the Universitat de Girona (Spain). All catalytic tests were done by duplicate.

IR data:

[1] H.-L. Chen, S. Dutta, P.-Y. Huang and C.-C. Lin, *Organometallics,* 2012, **31**, 2016.

[N,N'-bis(3,5-di-*tert*-butylsalicylene)-2-aminobenzyl-amino]chloridoaluminium(III) (1): Selected IR bands (ATR, ν, cm-1): 2952 m, 2904 m, 2868 m, 1615 ν(C=N) s, 1598 ν(C=N) m, 1554 m, 1540 s, 1387 m, 1360 m, 1257ν (C-O) s, 1230 ν (C-O) m, 1202 m, 1174 s, 1037 m, 842 s, 787 m, 763 s.

[N,N'-bis(3,5-di-*tert*-butylsalicylene)-2-aminobenzyl-amino]chloridoiron(III) (2): Selected IR bands (ATR, ν, cm^{-1}): 2950 m, 2903 m, 2866 m, 1608 ν(C=N) s, 1592 ν(C=N) s, 1549 m, 1534 s, 1437 m, 1385 m, 1359 m, 1317 m, 1271 m, 1254 ν(C-O) s, 1226 ν(C-O) m, 1171 s, 855 m, 838 s, 785 m, 758 s.

(Acetato-κ^2*O,O*)[N,N'-bis(3,5-di-*tert*-butylsalicylene)-2-aminobenzyl-amino]chloridocobalt (III) (3): Selected IR bands (ATR, ν,cm-1): 2953 m, 2899 m, 2861 m, 1613 ν(C=N) s, 1602 ν(C=N) m, 1547 m, 1525 s, 1447 s, 1460 m, 1428 m, 1409 m, 1257 ν(C-O) m, 1200 m, 1166 s, 1024 m, 949 m, 781 m, 761 m, 686 m.

Aqua[N,N'-bis(3,5-di-*tert*-butylsalicylene)-2-aminobenzyl-amino]chloridochromium(III) (4): Selected IR bands (ATR, ν, cm-1): 2952 m, 2904 m, 2868 m, 1611 ν(C=N) s, 1579, 1530 s, 1416 m, 1386 m, 1359 m, 1318 m, 1256 ν(C-O) s, 1225 ν(C-O) m, 1170 s, 1036 m, 837 s, 759 s.

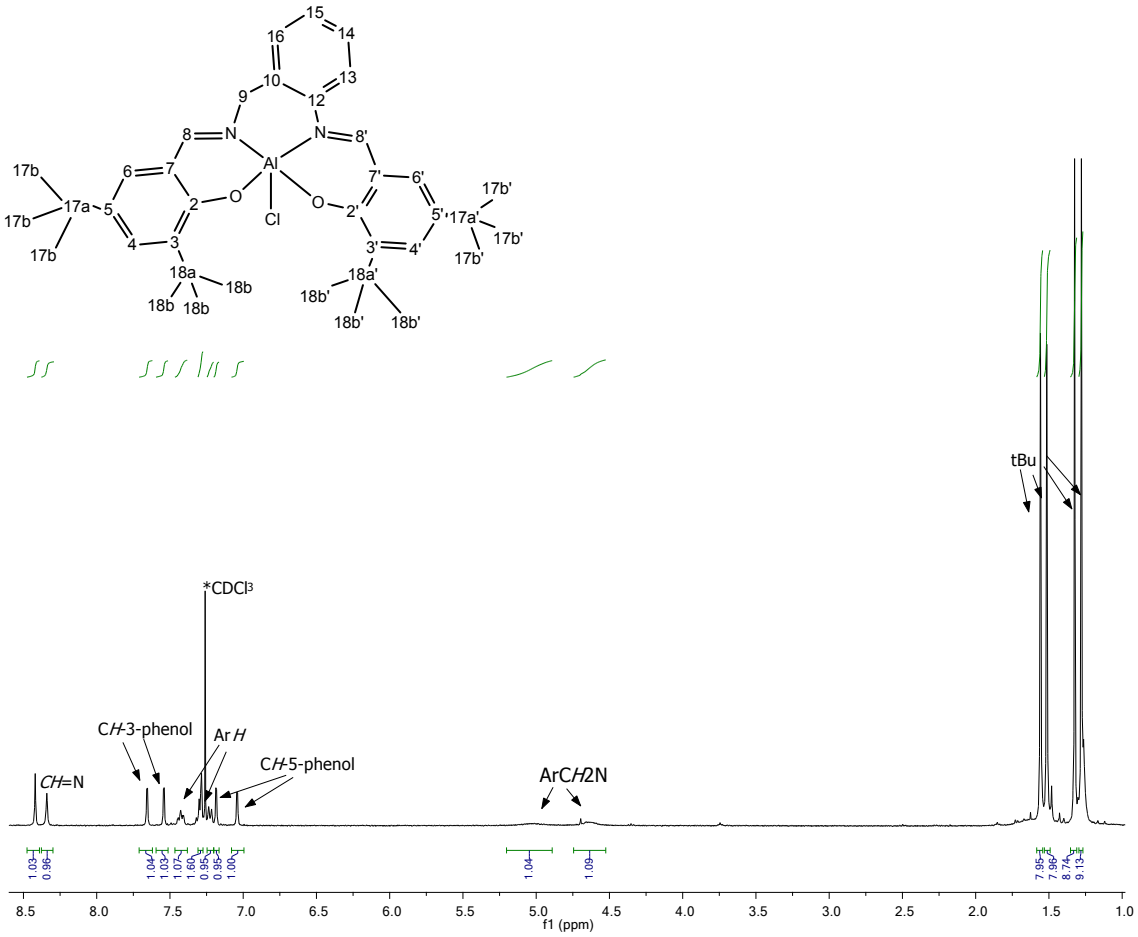

Figure S1. ^{1}H NMR spectrum of **1** in $CDCl_3$.

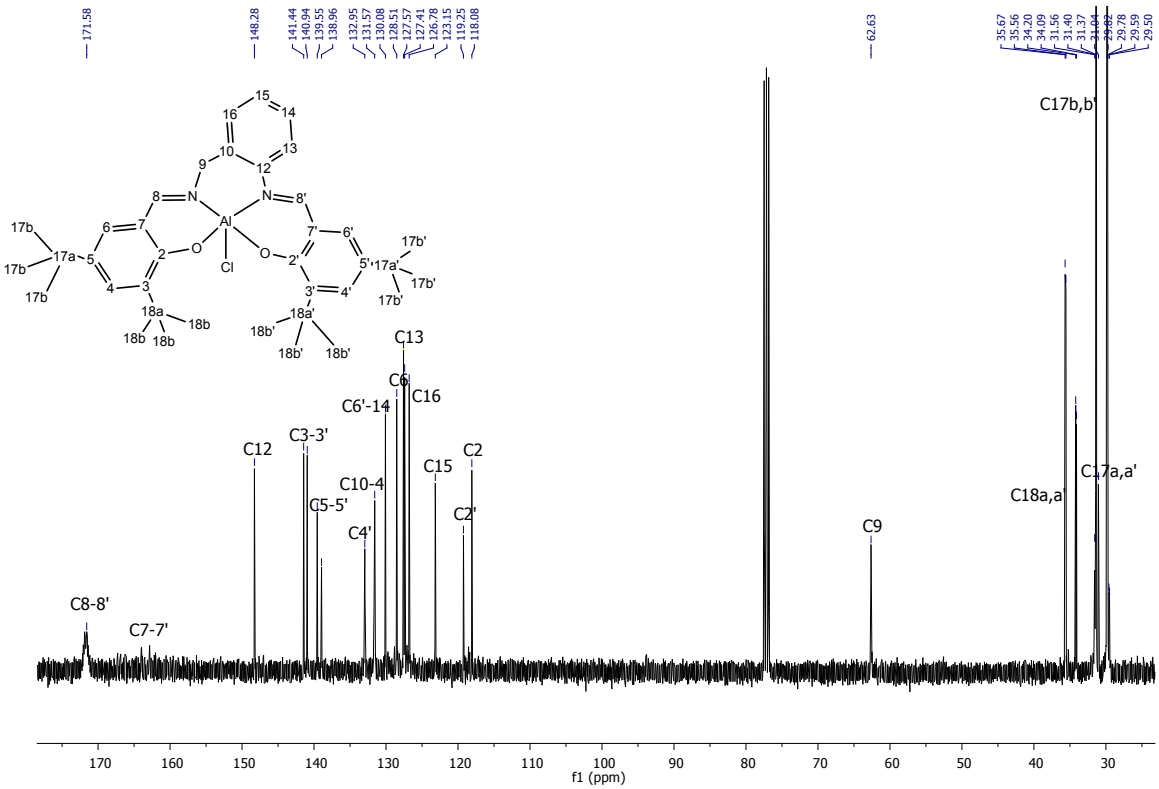

Figure S2. ^{13}C NMR spectrum of **1** in $CDCl_3$.

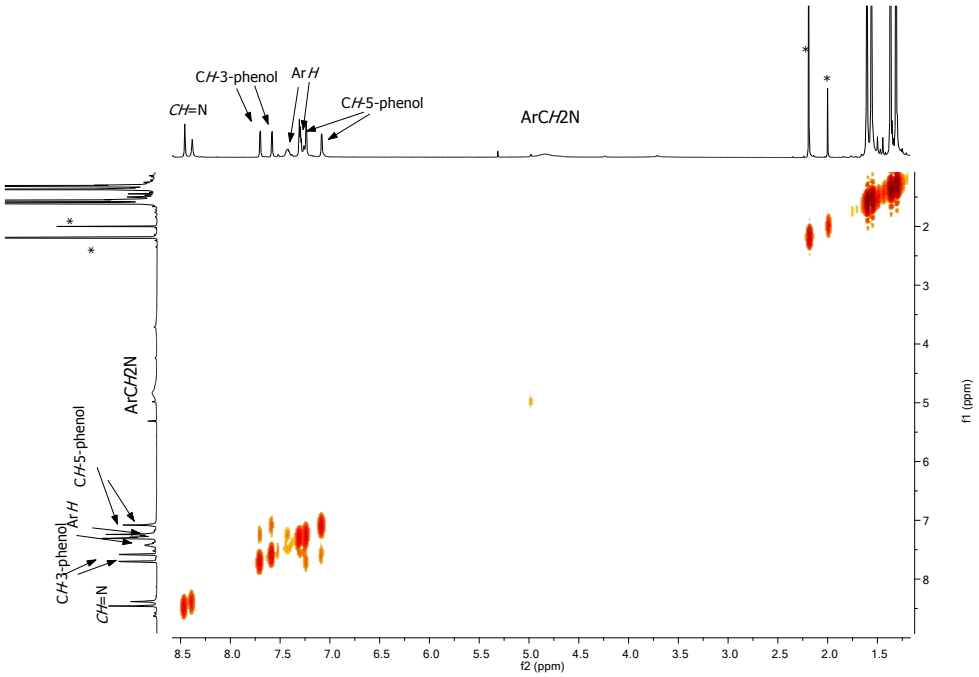

Figure S3. ^{1}H-^{1}H COSY NMR spectrum of **1** in $CDCl_3$.

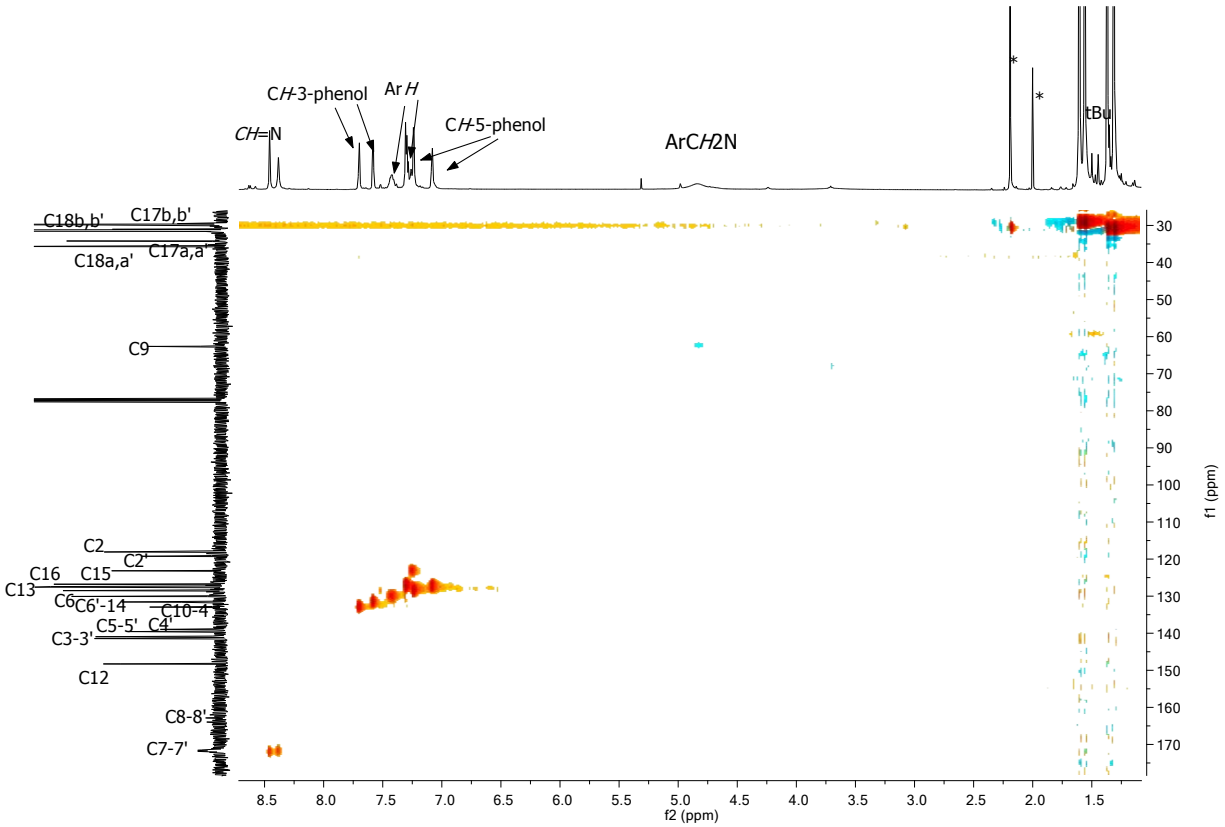

Figure S4. ^{1}H-^{13}C HSQC NMR spectra of **1** in $CDCl_3$.

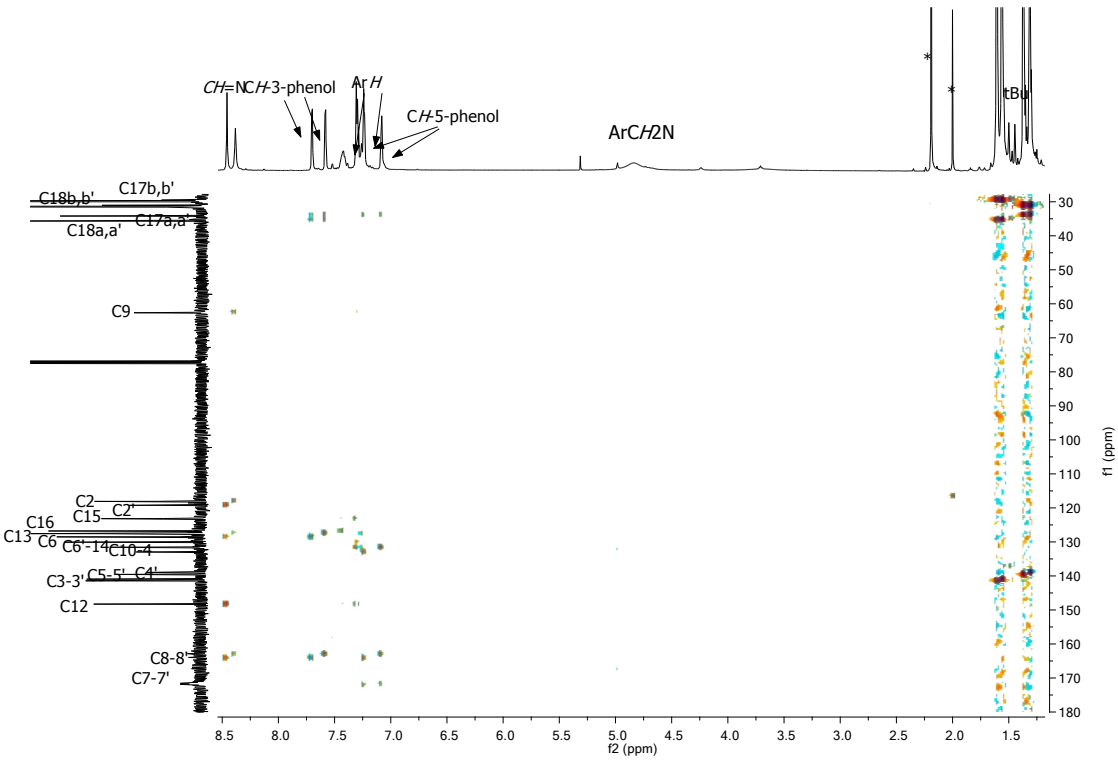

Figure S5. ^{1}H-^{13}C HMBC NMR spectra of **1** in $CDCl_3$.

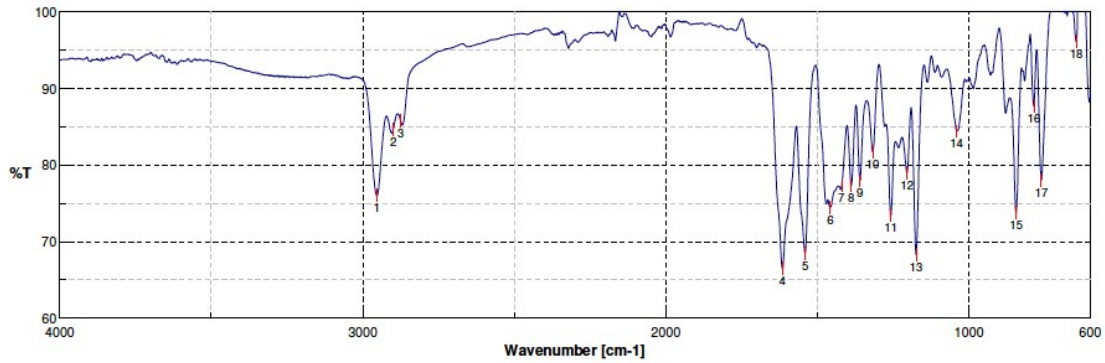

No.	cm-1	%T	No.	cm-1	%T	No.	cm-1	%T	No.	cm-1	%T	No.	cm-1	%T
1	2953.45	76.0201	2	2899.93	84.5870	3	2874.86	85.7307	4	1615.09	66.4747	5	1540.36	68.5137
6	1456.96	74.4959	7	1419.83	77.2534	8	1388.01	77.3100	9	1359.09	77.9432	10	1317.14	81.7147
11	1257.84	73.4207	12	1204.33	78.9817	13	1173.95	68.3492	14	1039.93	84.4204	15	844.186	73.8177
16	785.368	87.6825	17	760.78	78.0350	18	645.554	96.0685						

Figure S6. IR spectrum of **1** in ATR (4000-600 cm^{-1}).

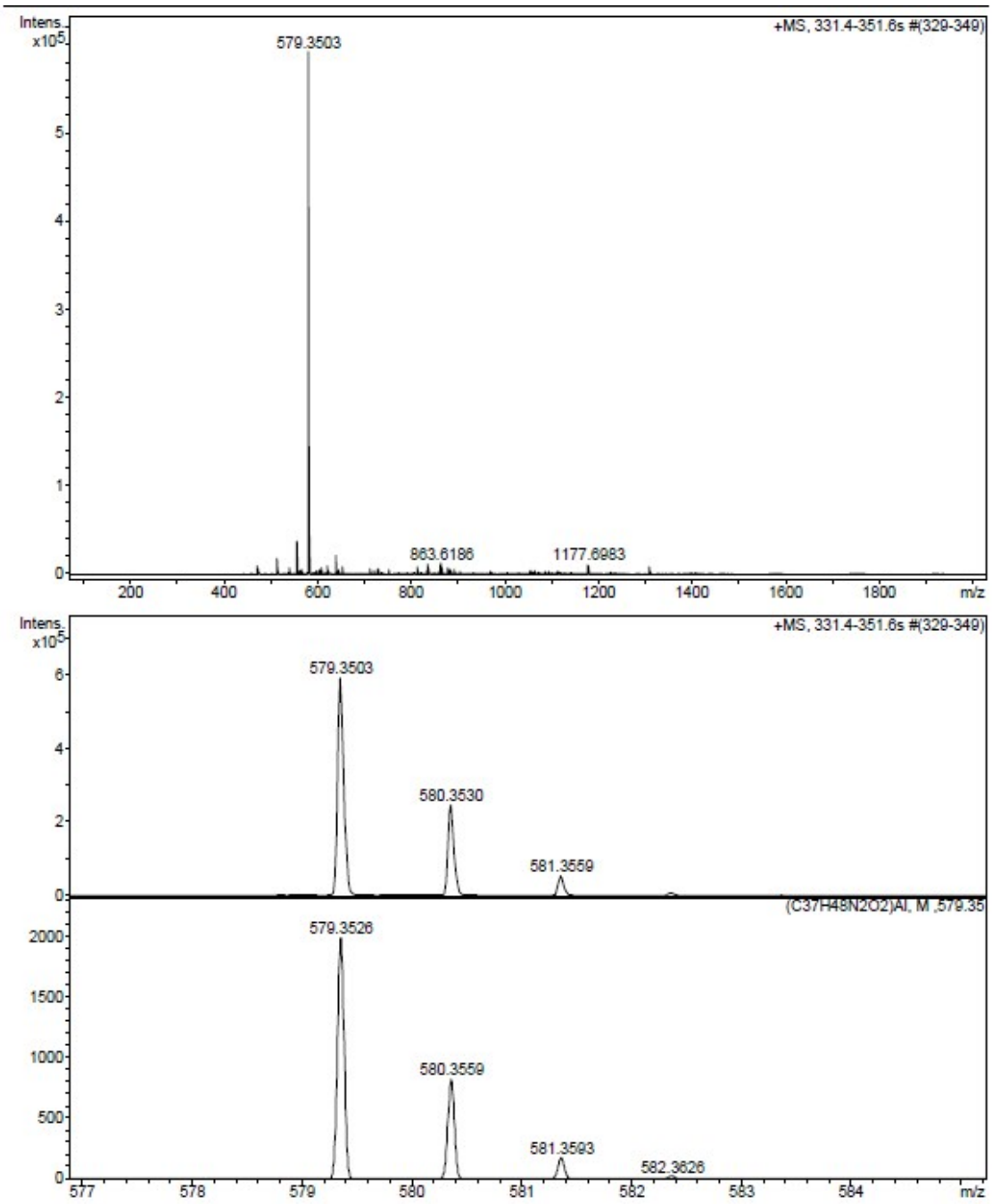

Figure S7. HRMS (ESI) spectrum of **1**.

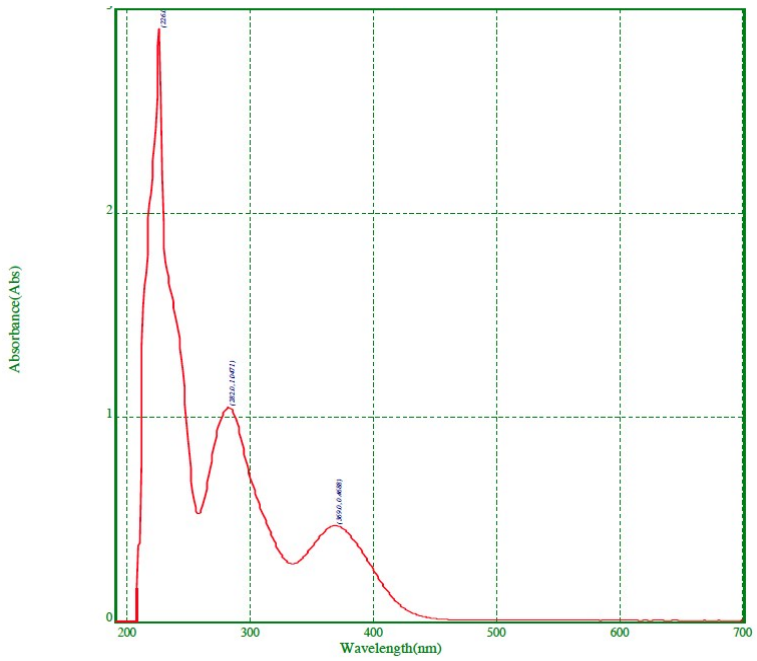

Figure S8. UV-visible spectrum of **1** in CH_3CN ($2.5 \cdot 10^{-5}$ M).

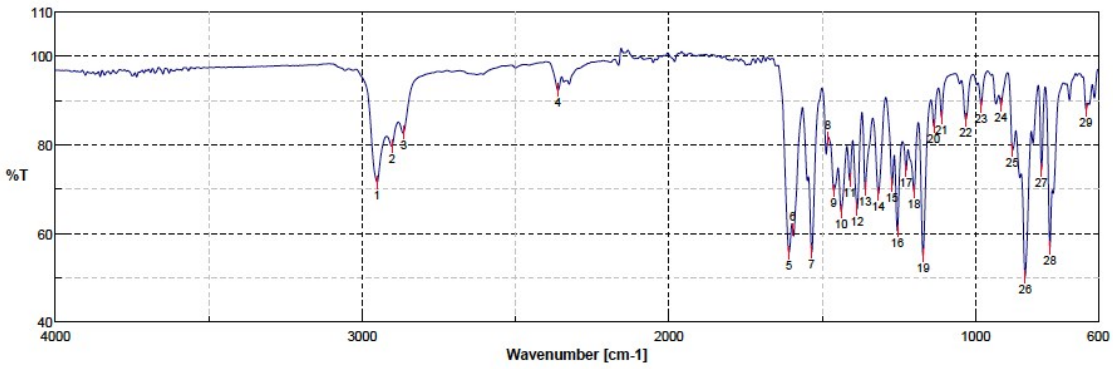

No.	cm-1	%T	No.	cm-1	%T	No.	cm-1	%T	No.	cm-1	%T	No.	cm-1	%T
1	2950.55	71.6325	2	2902.34	79.8386	3	2864.74	82.7903	4	2361.41	92.3648	5	1608.34	55.7052
6	1595.81	60.9325	7	1534.1	55.9049	8	1481.06	81.5285	9	1461.78	69.6932	10	1437.67	64.9966
11	1409.71	71.9947	12	1385.6	65.6017	13	1359.57	70.0275	14	1316.18	69.0076	15	1271.82	70.9403
16	1254.47	60.6215	17	1226.5	74.301	18	1200.47	69.4589	19	1170.58	55.1445	20	1135.87	84.1848
21	1110.8	86.295	22	1031.73	85.7548	23	981.59	88.8712	24	916.986	88.973	25	879.381	78.7914
26	837.919	50.3702	27	784.886	74.4366	28	756.923	56.9229	29	639.287	87.9506			

Figure S9. IR spectrum of **2** in ATR (4000-600 cm^{-1}).

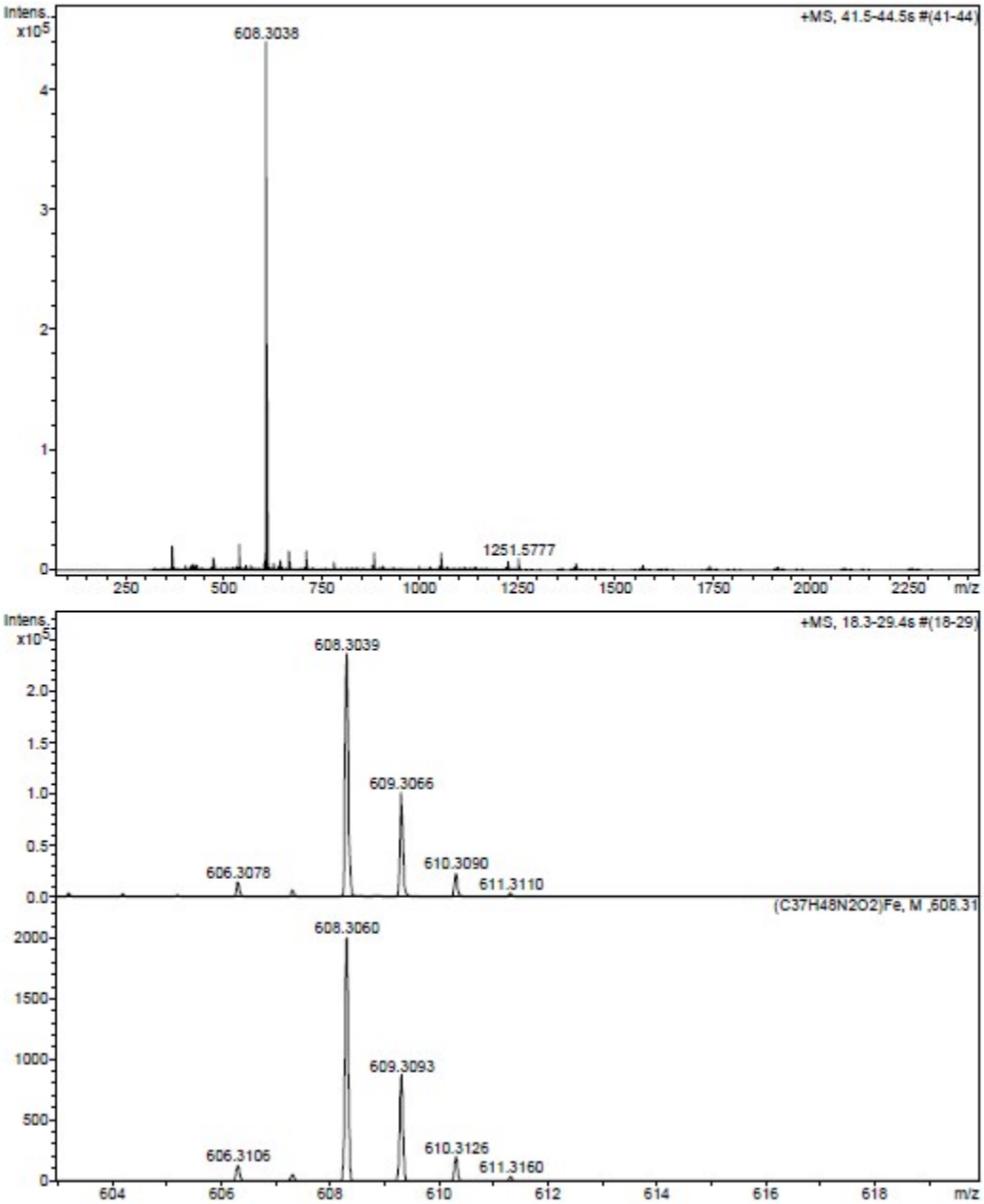

Figure S10. HRMS (ESI) spectrum of **2**.

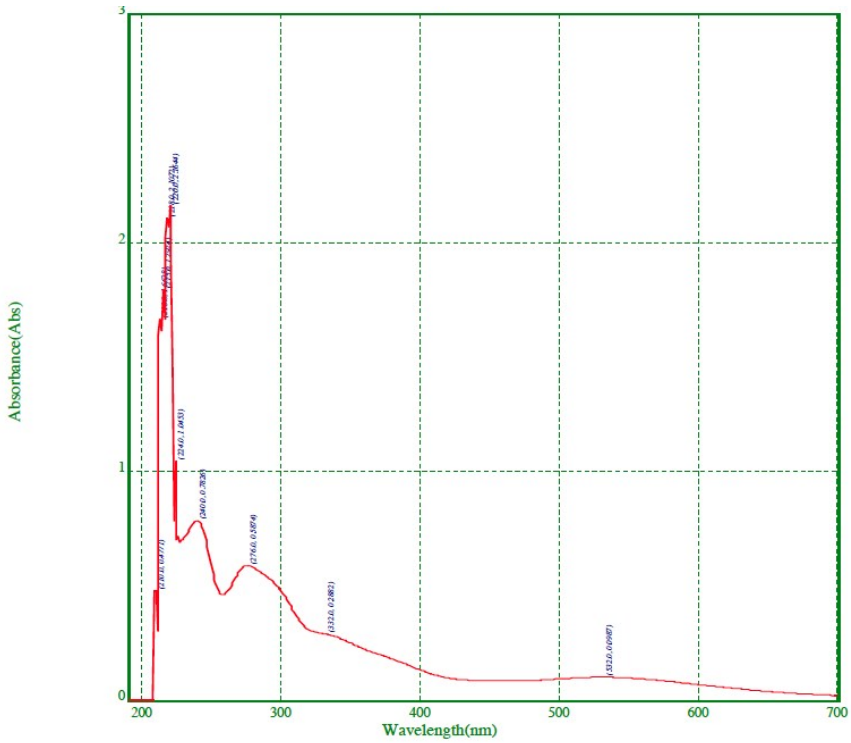

Figure S11. UV-visible spectrum of **2** in CH_3CN ($2.5 \cdot 10^{-5}$ M).

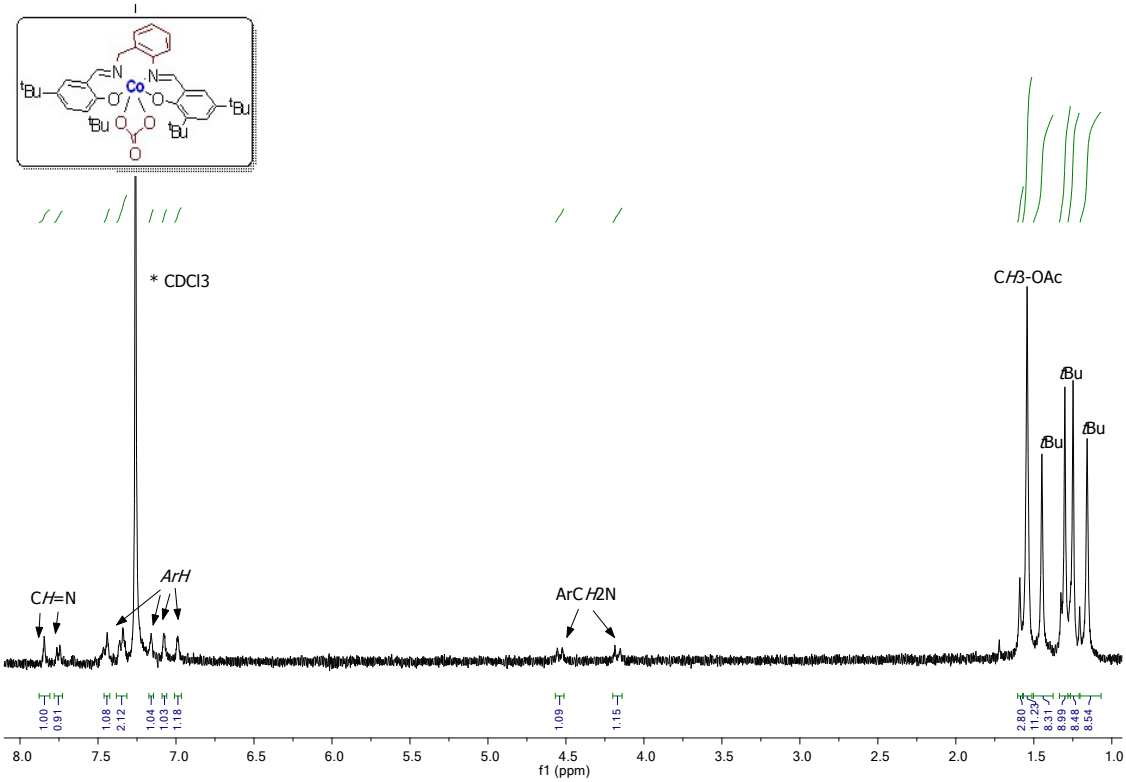

Figure S12. ^{1}H NMR spectrum of **3** in $CDCl_3$.

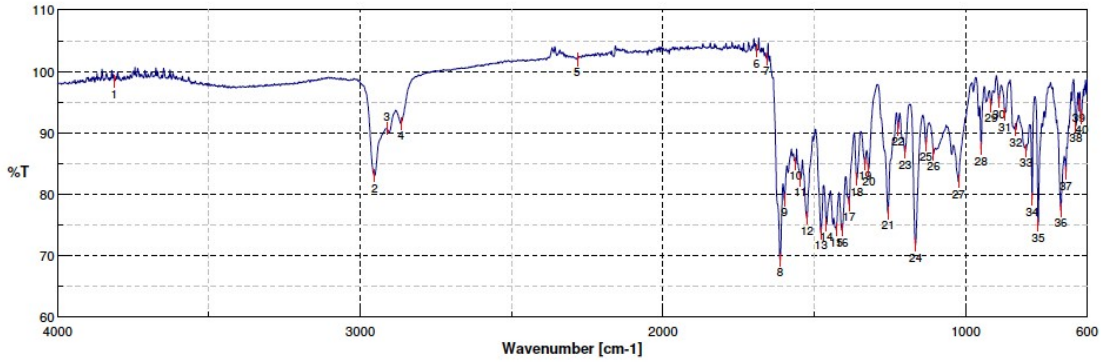

No.	cm-1	%T	No.	cm-1	%T	No.	cm-1	%T	No.	cm-1	%T	No.	cm-1	%T
1	3812.1	98.3535	2	2952.48	83.0435	3	2912.47	90.6583	4	2866.67	91.5319	5	2283.79	101.9523
6	1691.75	103.3223	7	1657.52	102.0871	8	1613.16	69.2808	9	1599.18	79.0489	10	1562.06	85.0096
11	1546.63	82.3786	12	1524.45	76.1229	13	1478.65	73.6780	14	1460.33	75.0670	15	1428.03	74.1916
16	1409.23	74.1568	17	1385.6	78.3359	18	1359.57	82.4847	19	1333.05	85.0027	20	1321	84.0501
21	1257.36	76.9459	22	1224.09	90.6187	23	1200.95	86.8596	24	1166.24	71.6987	25	1132.01	88.1406
26	1106.94	86.5818	27	1024.5	82.0593	28	949.77	87.4032	29	916.986	94.4673	30	890.952	95.1041
31	871.185	92.9816	32	835.026	90.4496	33	800.796	87.0873	34	781.029	79.1777	35	761.262	74.9344
36	686.534	77.3825	37	669.178	83.3512	38	636.394	91.1543	39	628.198	94.5011	40	617.592	92.5321

Figure S13. IR spectrum of **3** in ATR (4000-600 cm^{-1})

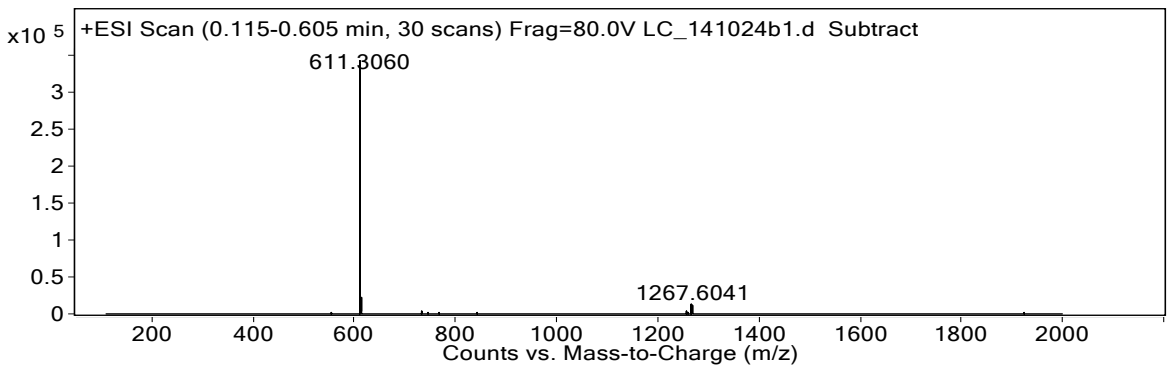

Figure S14. HRMS (ESI) spectrum of **3**.

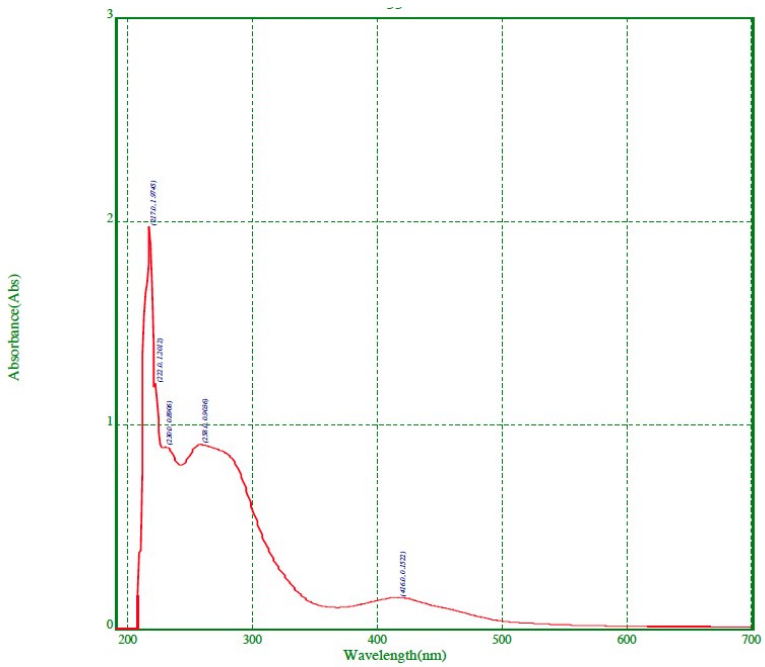

Figure S15. UV-visible spectrum of **3** in CH_3CN ($2.5 \cdot 10^{-5}$ M).

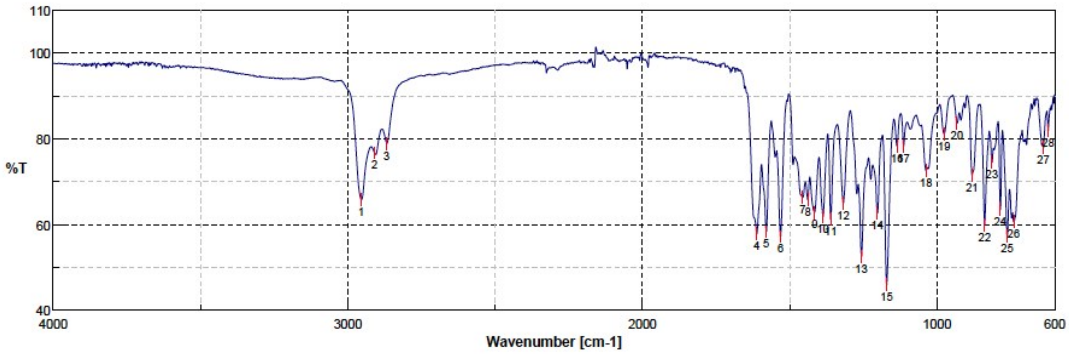

No.	cm-1	%T	No.	cm-1	%T	No.	cm-1	%T	No.	cm-1	%T	No.	cm-1	%T
1	2953.93	65.8229	2	2909.09	76.7468	3	2867.63	78.9875	4	1611.23	57.8738	5	1578.93	58.3886
6	1530.72	57.2736	7	1455.51	66.3936	8	1437.67	65.7667	9	1415.01	62.874	10	1386.57	61.8652
11	1360.05	61.2765	12	1317.63	65.0515	13	1255.91	52.5234	14	1201.43	62.7401	15	1170.58	46.0127
16	1135.38	78.3694	17	1112.73	78.309	18	1037.03	72.6431	19	974.84	81.2031	20	931.45	83.6651
21	880.345	71.5616	22	837.919	59.8739	23	812.849	74.5534	24	784.404	63.545	25	761.262	57.4791
26	739.085	60.7052	27	638.323	77.9288	28	621.931	81.927						

Figure S16. IR spectrum of **4** in ATR (4000-600 cm^{-1}).

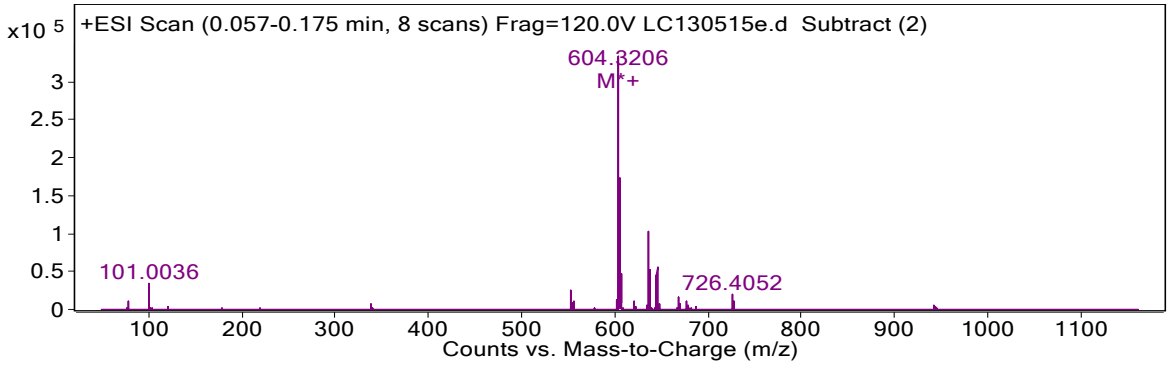

Figure S17. HRMS (ESI) spectrum of **4**.

Table S1. Crystallographic data and details of structure refinement for compounds **2-4**

	2	**3**	**4**
Molecular formula	$C_{78}H_{106}Cl_2Fe_2N_4O_5$	$C_{39}H_{51}CoN_2O_4$	$C_{43}H_{62}ClCrN_2O_{4.50}$
Molecular weight	1362.26	670.74	766.39
Crystal system	Monoclinic	Monoclinic	Monoclinic
Space group	C2/c	P2(1)/n	C2/c
Temp. (K)	100(2)	100(2)	100(2)
Radiation (λ, Å)	Mo Kα (λ=0.71073 Å)	Mo Kα (λ=0.7107 Å)	Mo Kα (λ=0.7107 Å)
a (Å)	19.0813(14	13.1775(8)	30.732(5)
b (Å)	19.8561(16)	23.4462(15)	12.284(2)
c (Å)	20.3191(13)	13.3026(8)	26.514(4)
α (º)	90	90	90
β (º)	101.408(3)	117.093(2)	120.596(4)
γ (º)	90	90	90
Volume (Å3)	7546.4(10)	3659.0(4)	8616(2)
Z	4	4	8
Dx (Mg·m-3)	1.199	1.218	1.182
F (000)	2912	1432	3288
Crystal dimensions (mm)	0.03 x 0.02 x 0.01	0.40 x 0.30 x 0.30	0.10 x 0.10 x 0.02
μ (Mo Kα) (mm-1)	1.686	1.737	1.661
θmax (º)	27.930	25.421	25.042
Reflections collected	28962	-	24685
Unique reflections	8355	6677	7609
Rint.	0.0479	0.0492	0.1115
Parameters	524	756	562
R1 [I >2σ(I)]	0.0477	0.0731	0.0920
wR2	0.1009	0.1982	0.1730
Δρ (e/ Å3)	0.517, -0.534	0.462, -0.510	0.459, -0.509

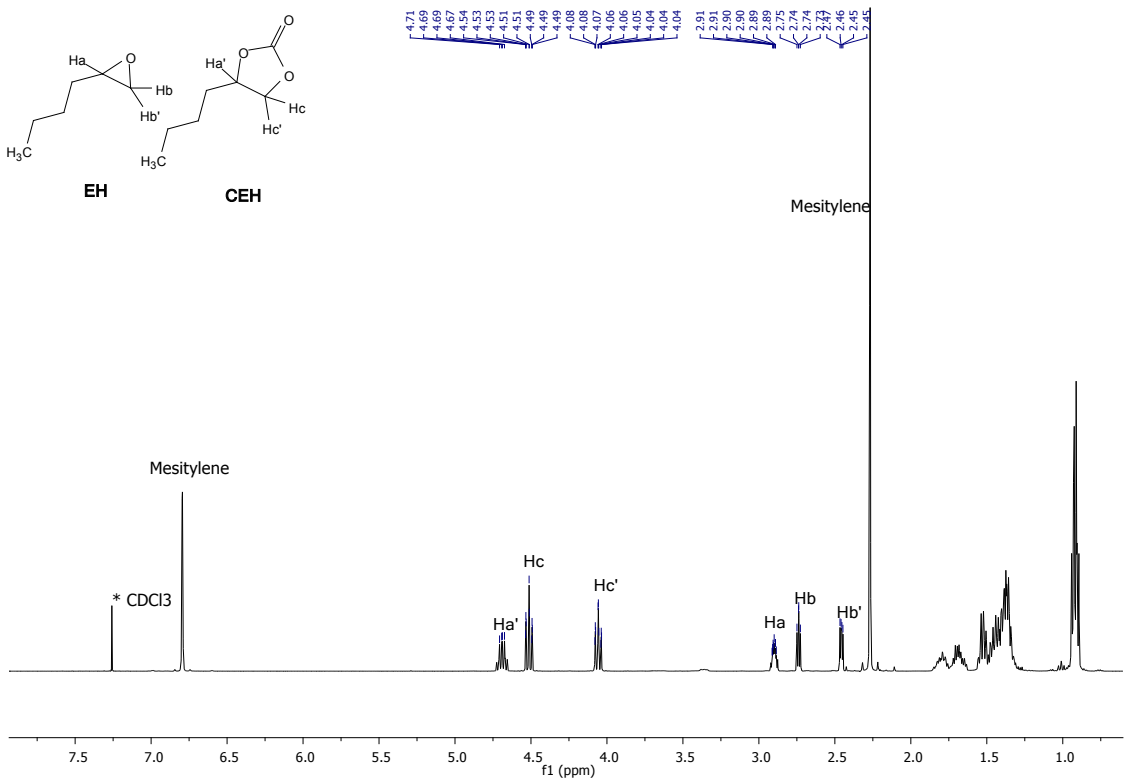

Figure S18. ^{1}H NMR spectrum in $CDCl_3$ of reaction crude using **1**/TBAB (entry 1, Table 2).

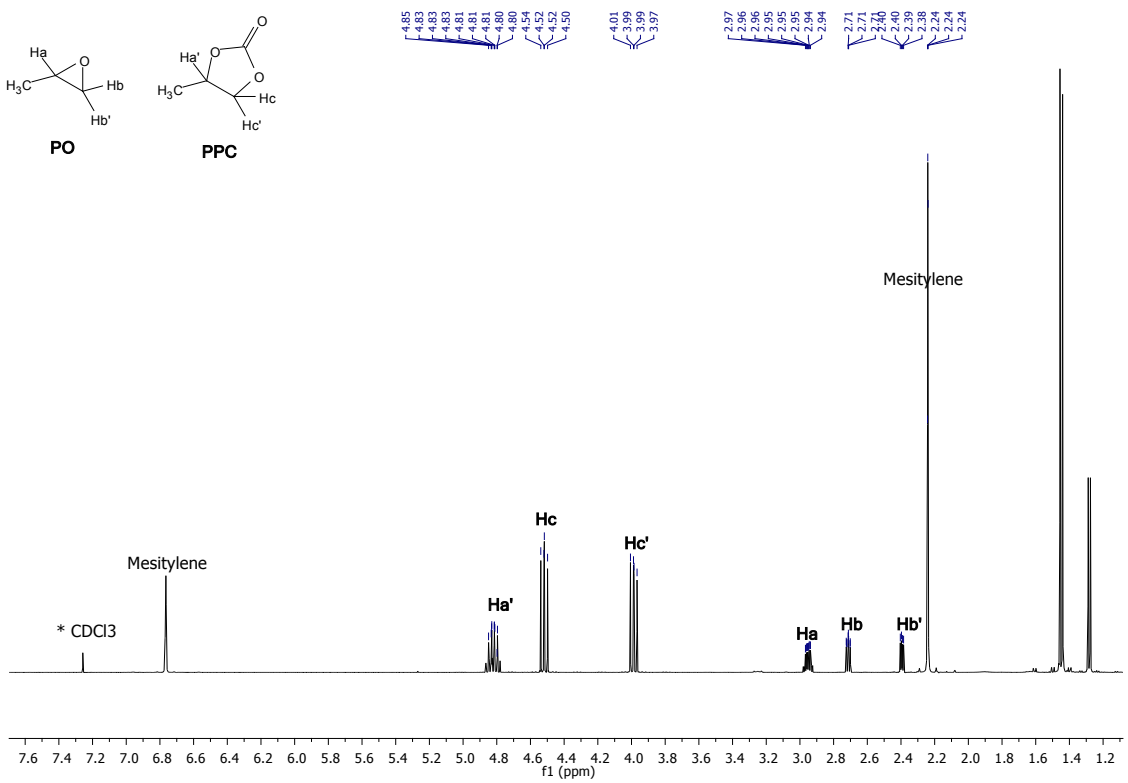

Figure S19. ^{1}H NMR spectrum in $CDCl_3$ of reaction crude using **1**/TBAB for the cycloaddition of CO_2 to propylene oxide (Figure 5).

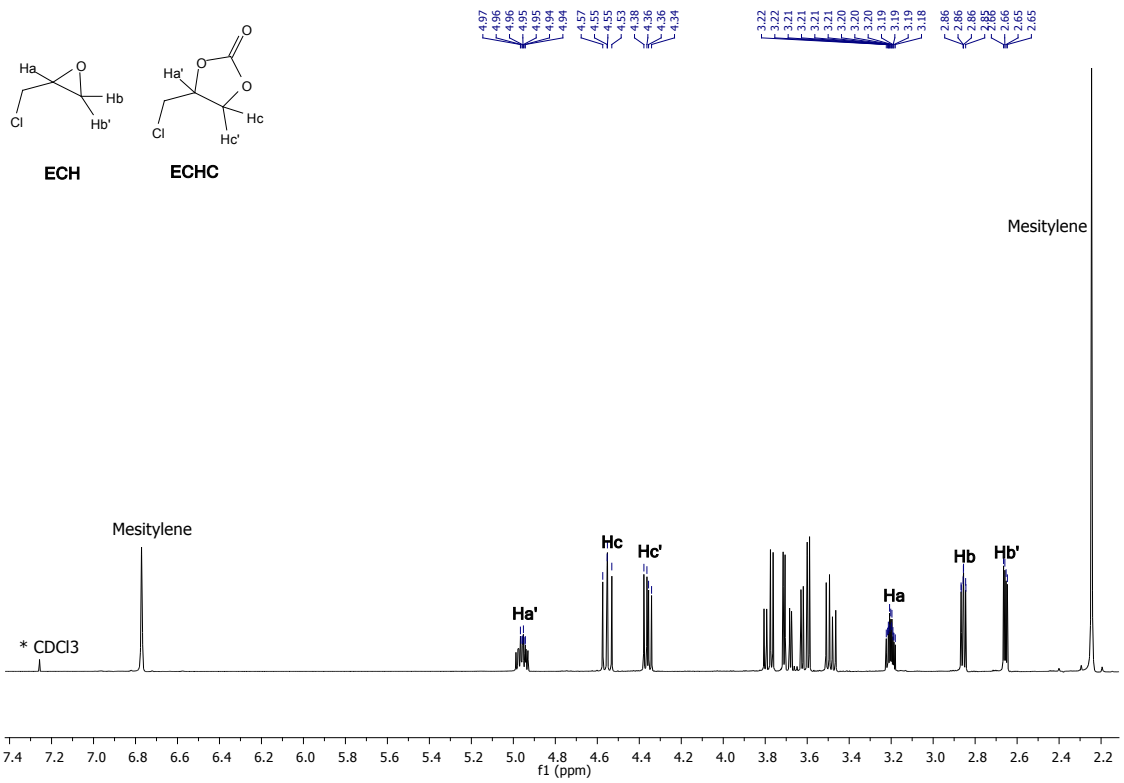

Figure S20.^{1}H NMR spectrum in $CDCl_3$ of reaction crude using **1**/TBAB for the cycloaddition of CO_2 to 1-chloro-2,3-epoxypropane (Figure 5).

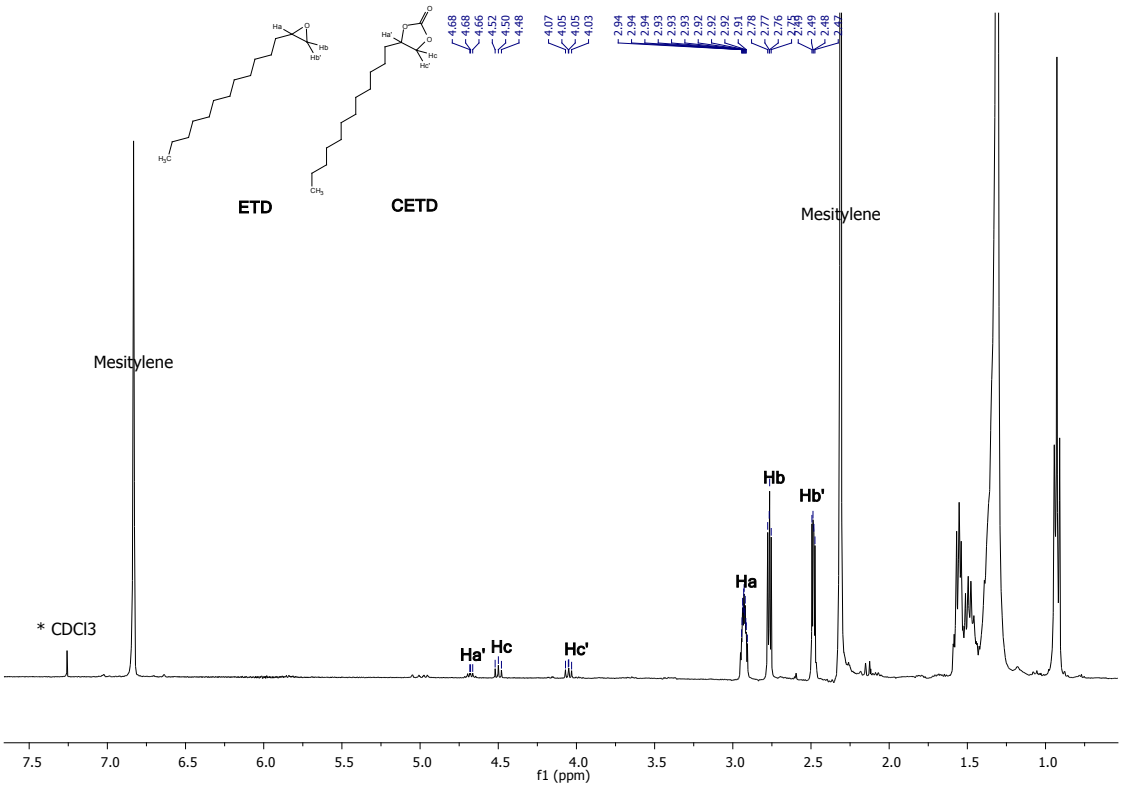

Figure S21.^{1}H NMR spectrum in $CDCl_3$ of reaction crude using **1**/TBAB for the cycloaddition of CO_2 to 1,2-epoxyteradecane (Figure 5).

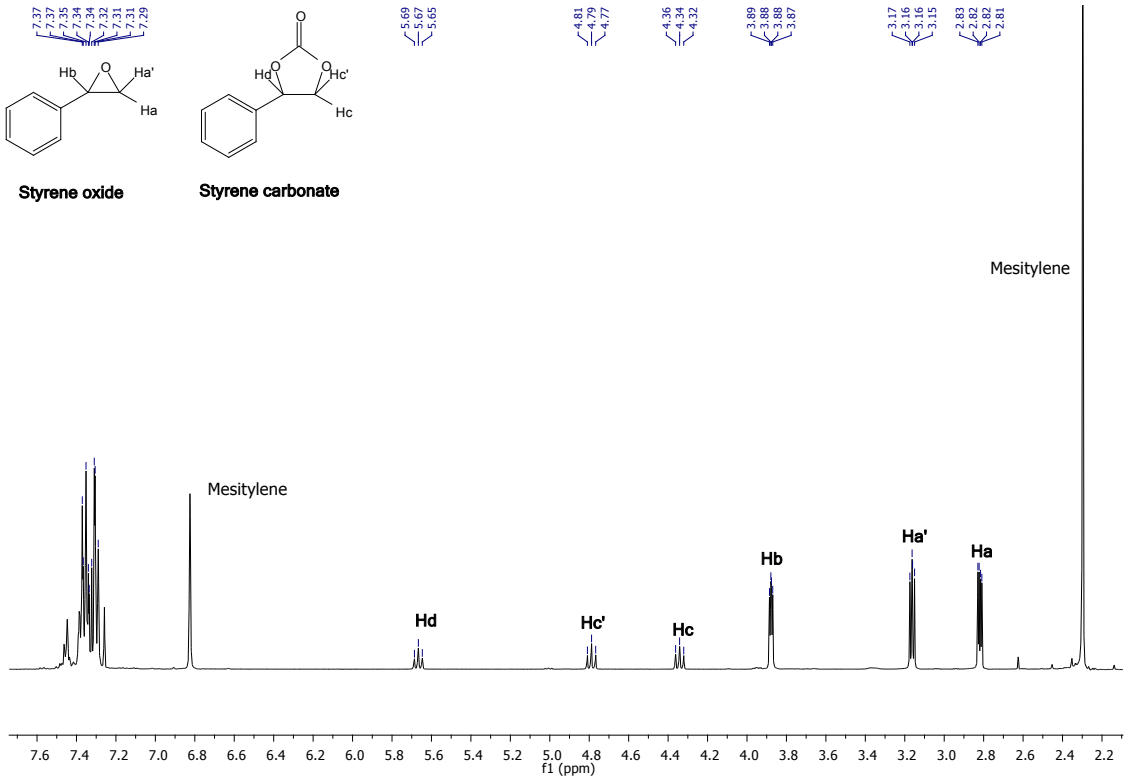

Figure S22. ^{1}H NMR spectrum in $CDCl_3$ of reaction crude using **1**/TBAB for the cycloaddition of CO_2 to styrene oxide (Figure 5).

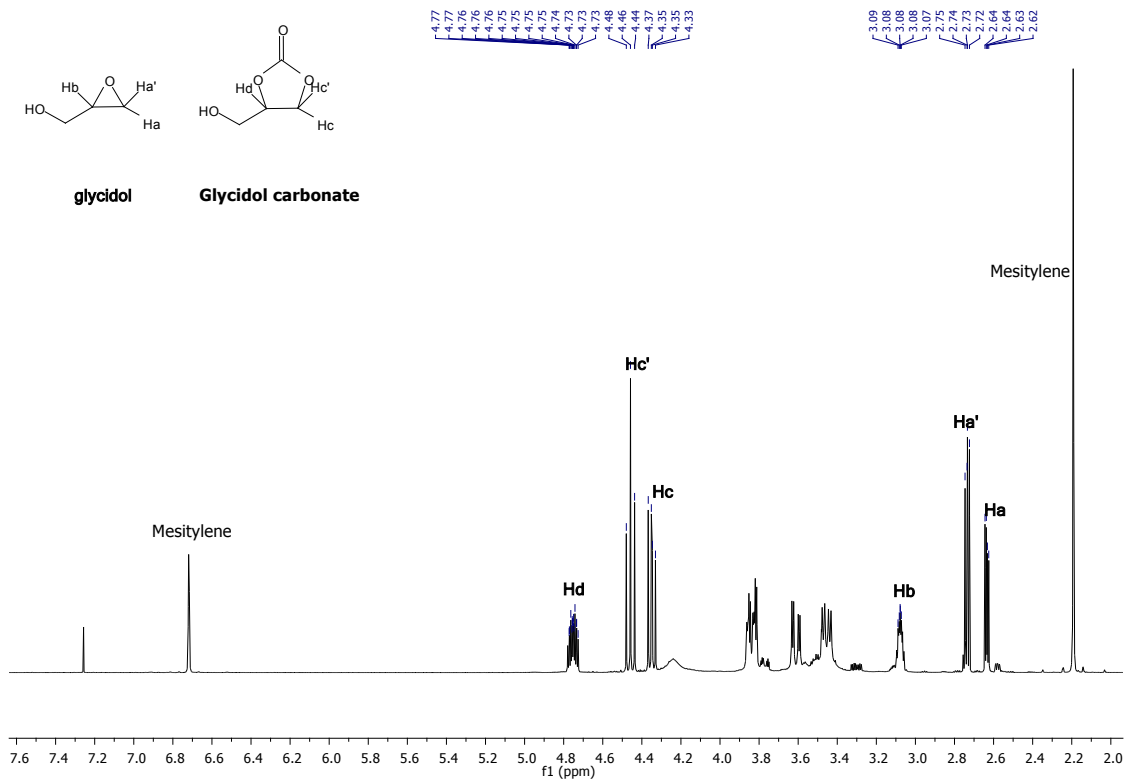

Figure S23. ^{1}H NMR spectrum in $CDCl_3$ of reaction crude using **1**/TBAB for the cycloaddition of CO_2 to glycidol (Figure 5).

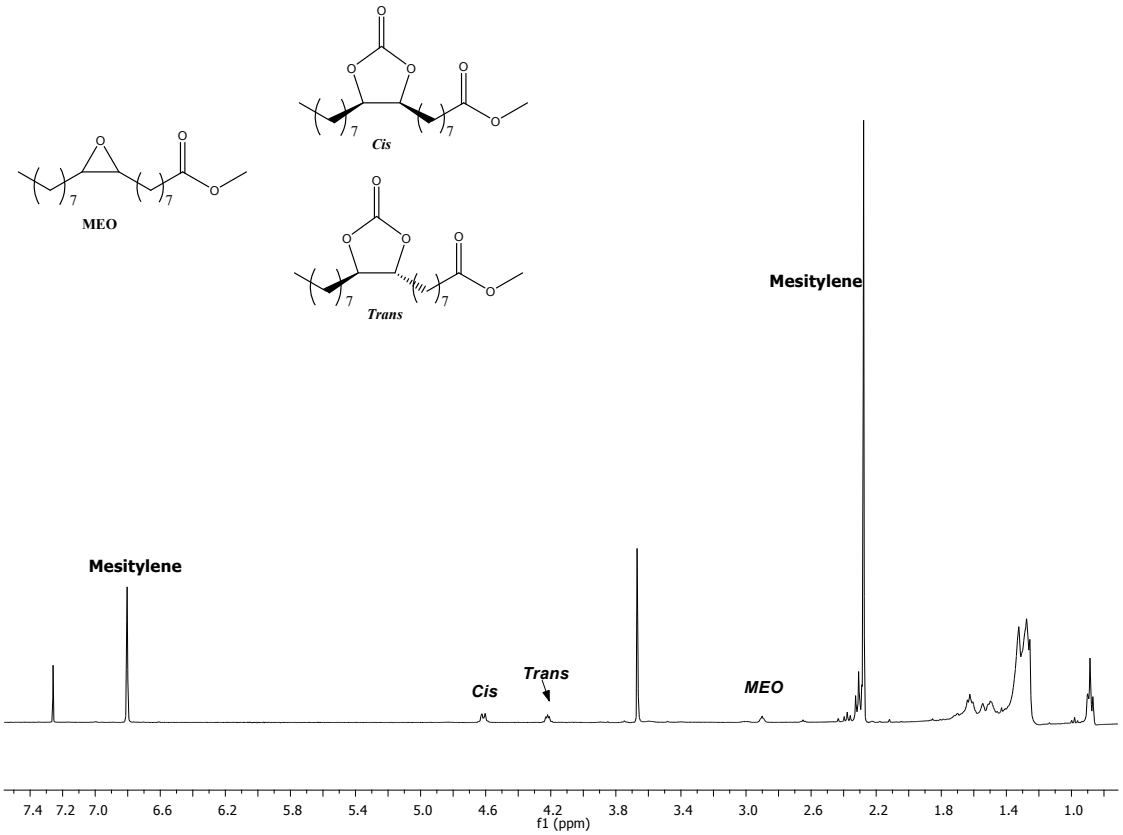

Figure S24. ^{1}H NMR spectrum in $CDCl_3$ of reaction crude using **1**/TBAB for the cycloaddition of CO_2 to methyl epoxioleate (Figure 5).

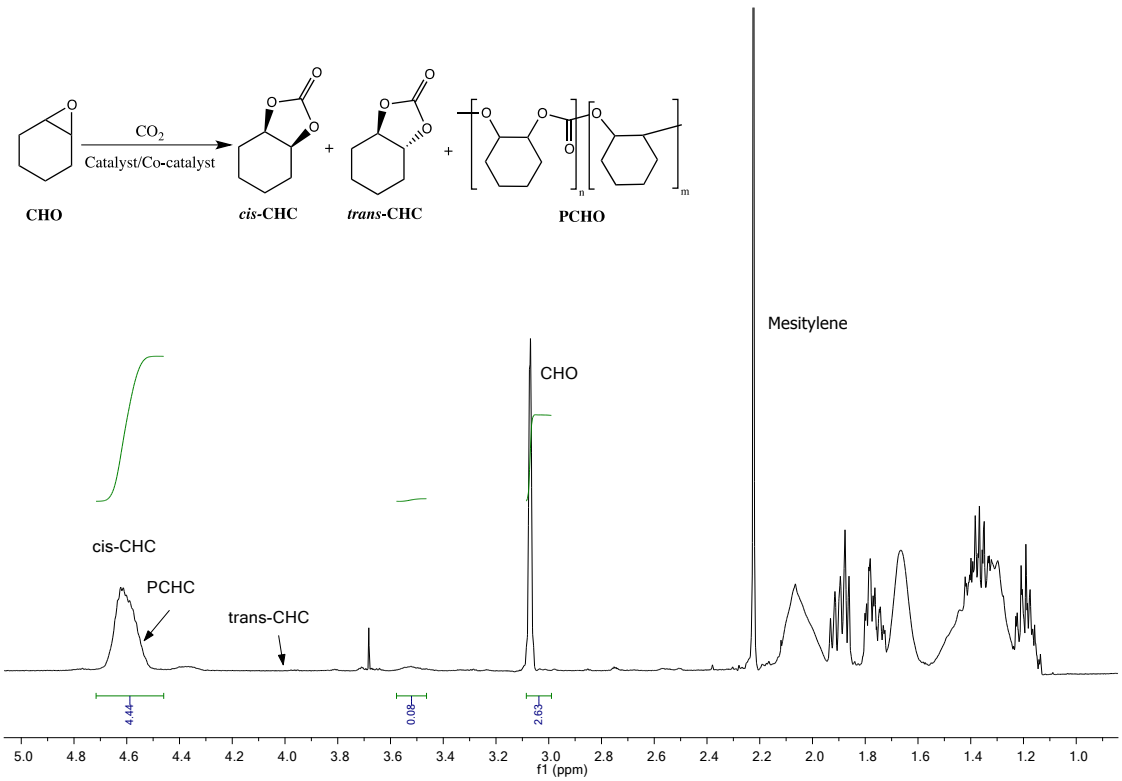

Figure S25. ^{1}H NMR spectrum in $CDCl_3$ of reaction crude using **1**/PPNCl for the coupling of CO_2 to cyclohexene oxide (entry 2, Table 3).

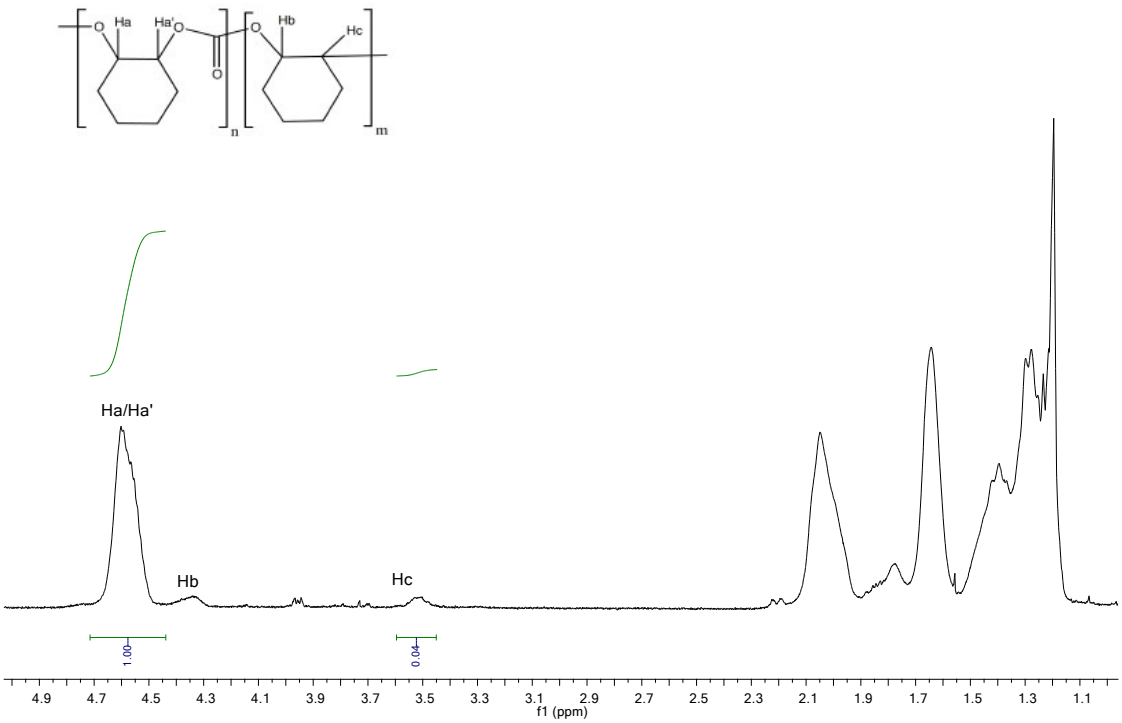

Figure S26. ^{1}H NMR spectrum in $CDCl_3$ of pure polycarbonate obtained using **1**/PPNCl from CO_2 and cyclohexene oxide (entry 2, Table 3).

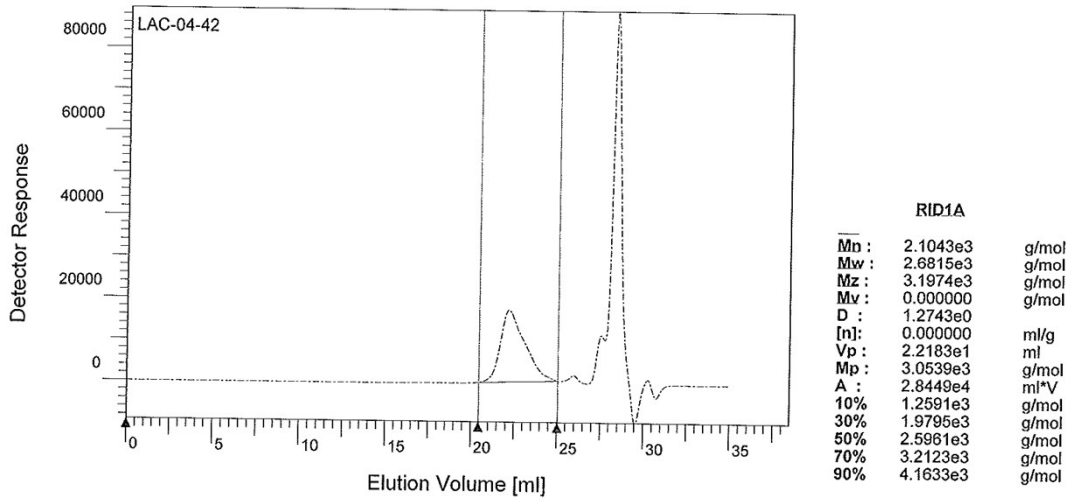

Figure S27. GPC chromatogram of PCHC obtained using **1**/PPNCl (entry 3, Table 3).

Kinetic studies

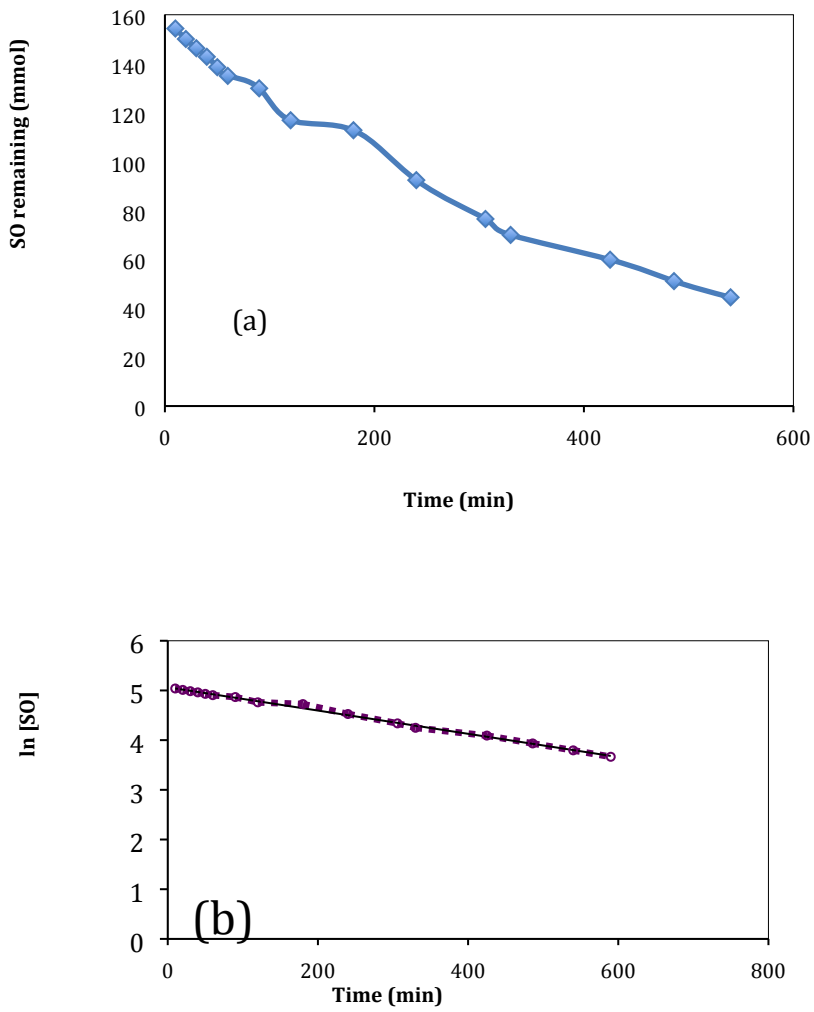

Fig. S28 (a) Styrene oxide conversion for **1**/TBAB catalytic system as a function of time. (b) Pseudo-first order kinetic plot of styrene oxide concentration against time for the **1**/TBAB catalytic system. Reaction conditions: T = 80 ºC, P_{CO2} = 10 bar, TBAB 0.2 mol %, catalyst 0.2 mol %.

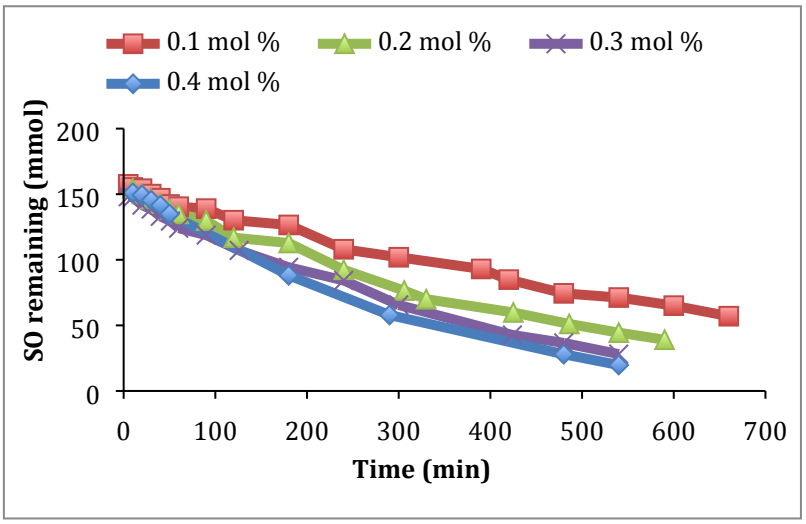

Figure S29. Styrene oxide conversion using **1**/TBAB catalytic system as a function of time at four different concentrations of **1**. Reaction conditions: T = 80 ºC, P_{CO2} = 10 bar, TBAB 0.2 mol %, catalyst 0.1-0.4 mol%.

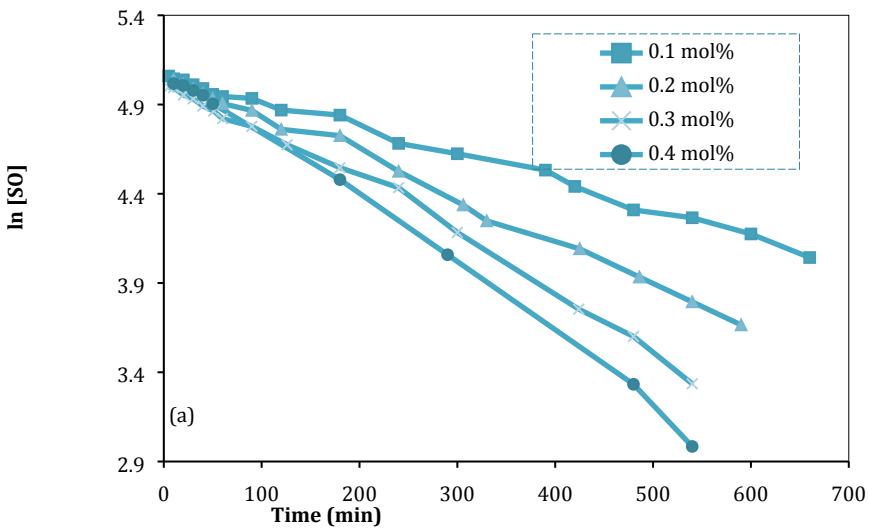

Figure S30. Logarithm of styrene oxide conversion using **1**/TBAB catalytic system as a function of time at four different concentrations of **1**. Reaction conditions: T = 80 ºC, P_{CO2} = 10 bar, TBAB 0.2 mol %, catalyst 0.1-0.4 mol%.

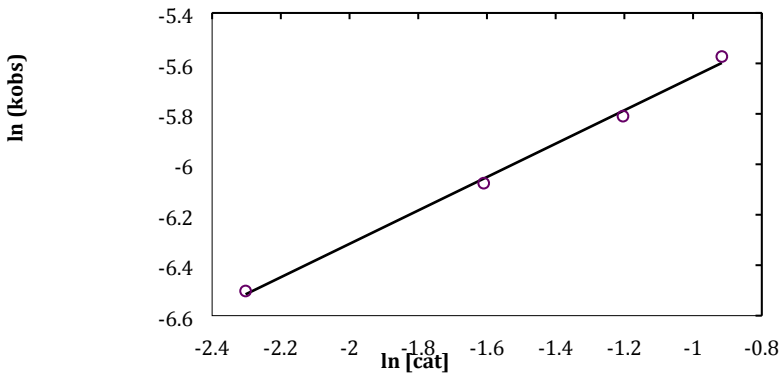

Figure S31. Double logarithm plot of ln (k_{obs}) respect to ln [**1**] at for different concentrations of **1** (0.1-0.4 mol %). Reaction conditions: T = 80 ºC, P_{CO2} = 10 bar, TBAB 0.2 mol %, catalyst 0.1-0.4 mol%.

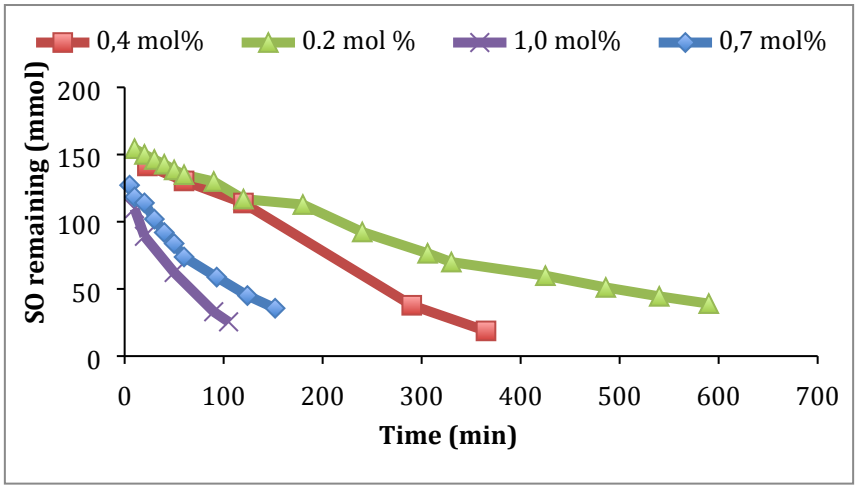

Figure S32. Styrene oxide conversion for the **1**/TBAB catalytic system as a function of time at four different concentrations of TBAB. Reaction conditions: T = 80 ºC, P_{CO2} = 10 bar, catalyst 0.2 mol %, TBAB 0.2-1.0 mol %.

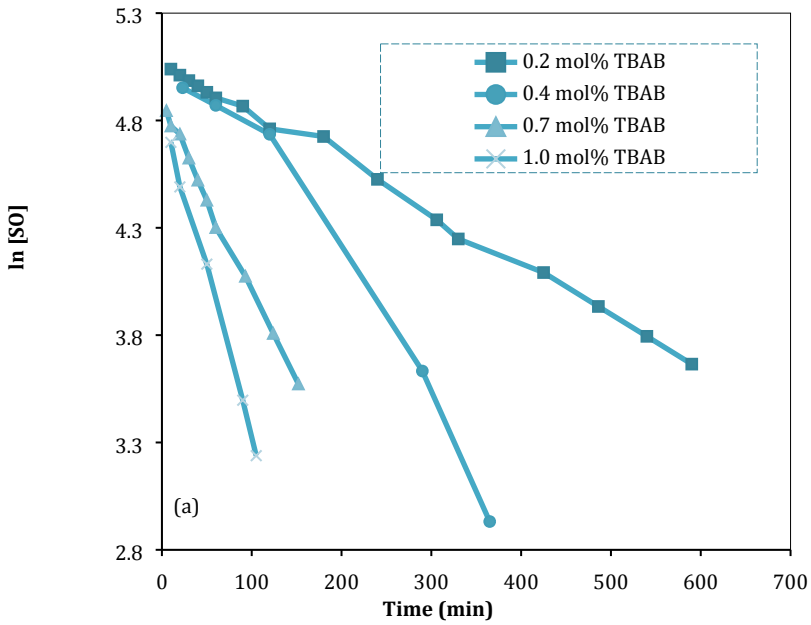

Figure S33. Logarithm of styrene oxide conversion for the **1**/TBAB catalytic system as a function of time at four different concentrations of TBAB. Reaction conditions: T = 80 ºC, P_{CO2} = 10 bar, catalyst 0.2 mol %, TBAB 0.2-1.0 mol %.

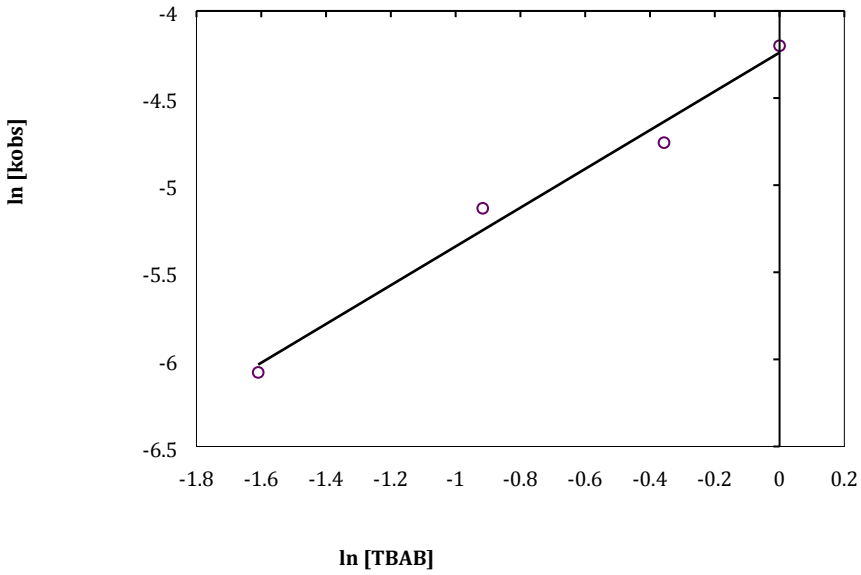

Figure S34. Double logarithm plot of ln (k_{obs}) respect to ln [TBAB] at four different concentrations of TBAB (0.2-1.0 mol %). Reaction conditions: T = 80 ºC, P_{CO2} = 10 bar, catalyst 0.2 mol %, TBAB 0.2-1.0 mol %.

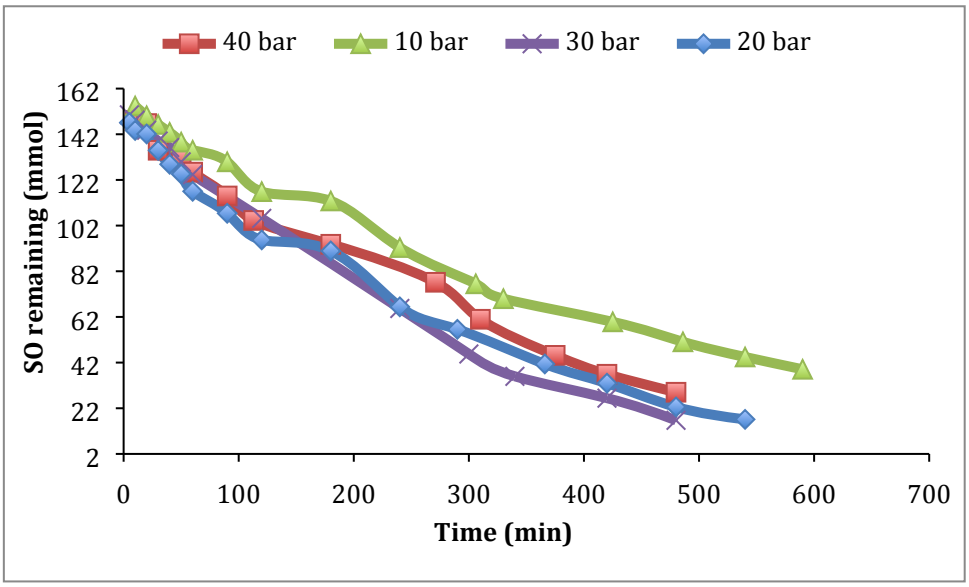

Figure S35. Styrene oxide conversion for the **1**/TBAB catalytic system as a function of time at four different CO_2 pressures. Reaction conditions: T = 80 ºC, catalyst 0.2 mol %, TBAB 0.2 mol %.

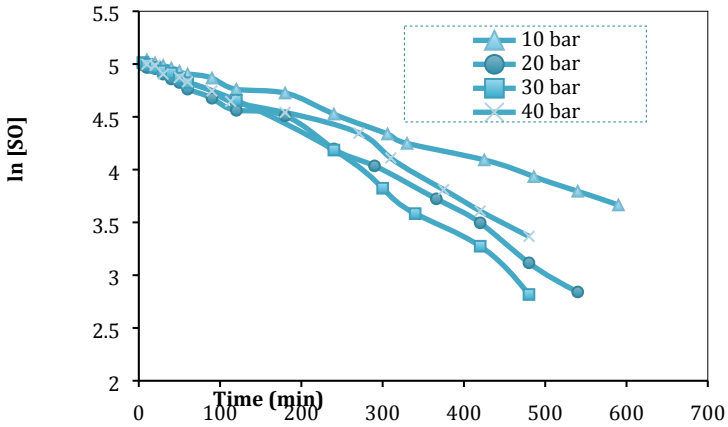

Figure S36. Logarithm of styrene oxide conversion for the **1**/TBAB catalytic system as a function of time at four different CO_2 pressures. Reaction conditions: T = 80 ºC, catalyst 0.2 mol %, TBAB 0.2 mol %.

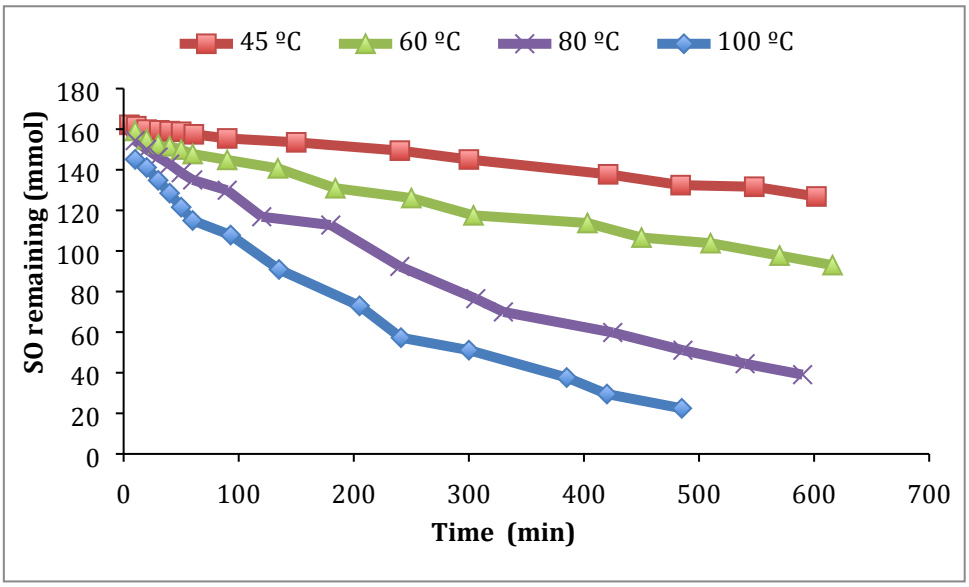

Figure S37. Styrene oxide conversion for the **1**/TBAB catalytic system as a function of time at four different temperatures. Reaction conditions: P_{CO2}: 10 bar, catalyst 0.2 mol %, TBAB 0.2 mol %.

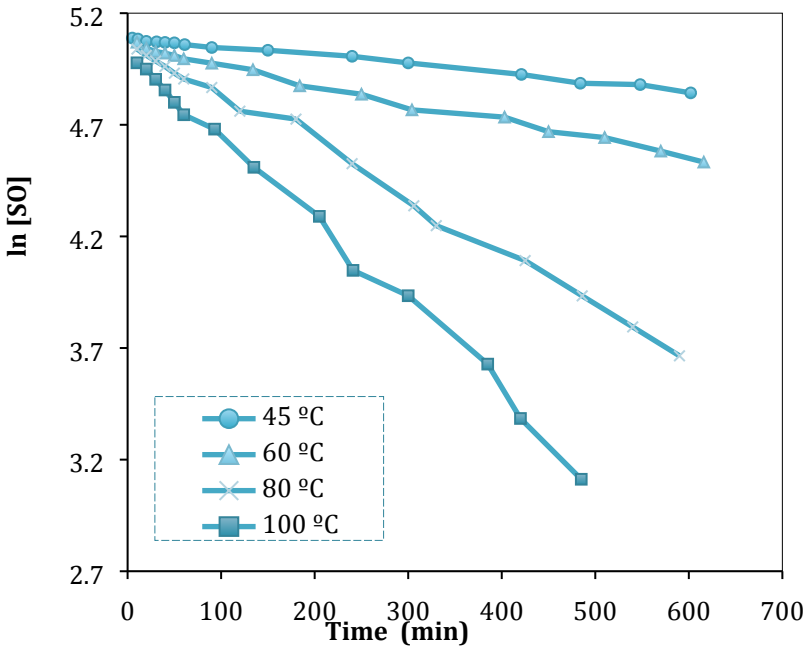

Figure S38. Logarithm of the styrene oxide concentration using **1**/TBAB catalytic system as a function of time at four different temperatures. Reaction conditions: P_{CO2}: 10 bar, catalyst 0.2 mol %, TBAB 0.2 mol %.

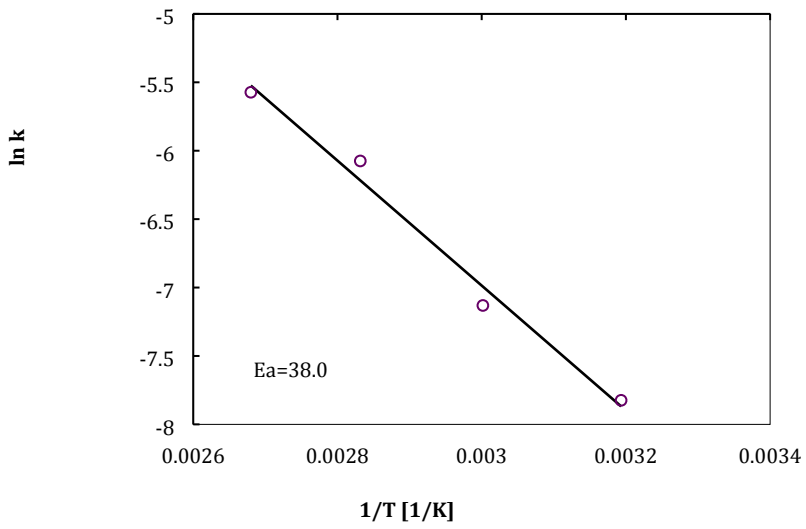

Figure S39. Arrehnius plot of the reaction of styrene oxide with CO_2 using **1**/TBAB as catalytic system. Reaction conditions: P_{CO2}: 10 bar, catalyst 0.2 mol %, TBAB 0.2 mol %.